Simulation studies of heavy ion heating by current-driven instabilities

M. Toida,[a] T. Maeda, I. Shiiba, A. Sugishima, and Y. Ohsawa
Department of Physics, Nagoya University, Nagoya 464-8602, Japan

(Received 22 June 2000; accepted 5 September 2000)

Nonlinear evolution of current-driven instabilities and associated energy transport among different particle species are studied by means of a two-dimensional, electrostatic, particle simulation code with full ion and electron dynamics. The plasma is assumed to consist of hydrogen (H) and helium (He) ions and electrons with the electron temperature larger than the ion temperatures; the electrons drift along a uniform magnetic field with an initial speed equal to the thermal speed. Then, simulations show that after the development of ion acoustic waves and fundamental H cyclotron waves, second harmonic waves are destabilized due to the change in the electron velocity distribution function parallel to the magnetic field, $f_e(v_\parallel)$. Even though the linear theory based on the initial conditions predicts that the second harmonics are only marginally unstable, they eventually grow to the largest amplitudes and heat He ions more significantly than H ions. The instabilities of these three kinds of modes with different phase velocities give rise to flattening of $f_e(v_\parallel)$ over a region larger than the thermal speed. © *2000 American Institute of Physics.* [S1070-664X(00)03612-0]

I. INTRODUCTION

Heating and acceleration of heavy ions are often observed in space plasmas. For instance, heavy ions as well as hydrogens are accelerated to high energies ($\gtrsim$MeV) in association with solar flares. The elemental compositions of these high-energy heavy ions are, on average, quite similar to those of the background solar coronal plasma.[1,2] This was demonstrated in simulations showing that a large-amplitude magnetosonic wave can accelerate all the heavy ions to nearly the same speed.[3,4] Also, in some solar flares, the abundance of ^{3}He is increased in energetic particles.[5–8] In those ^{3}He-rich events, the abundances of heavier ions such as Fe, Si, Mg, etc. also tend to increase.[9–11] Furthermore, in the Earth's ionosphere, oxygen ions, O^+, are known to be heated perpendicular to the geomagnetic field.[12–14]

Many of the events of heavy-ion energization remain unresolved. For the ^{3}He enrichment or O^+ heating, cyclotron resonances between particles and waves destabilized by electron currents are thought to play an essential role, and several theoretical models have been proposed.[15–21] However, theories quantitatively explaining the observations have not been established. To do this, we need to develop a theory which treats, in a self-consistent manner, both the nonlinear evolution of instabilities and energy transport among different particle species.

In this article, we study current-driven instabilities and associated energy transport in a plasma containing multiple ion species in a uniform magnetic field by using a two-dimensional (two space and three velocity components), electrostatic, particle simulation code with full ion and electron dynamics. We would like to investigate how instabilities grow and how the particles gain or lose energy in a multi-ion-species plasma. We are particularly interested in whether and how the heavy ions can be heated.

The plasma is assumed to have hydrogen and helium with the density ratio $n_{\mathrm{He}}/n_{\mathrm{H}}=0.1$, as in space plasmas.[2] The electrons drift along the magnetic field with the initial speed equal to the thermal speed, $v_{\mathrm{d}}=v_{\mathrm{Te}}$. The electron temperature is taken to be higher than the ion temperature, $T_{\mathrm{e}}=5T_{\mathrm{H}}$. In these circumstances, the linear theory which is presented in Sec. II predicts that ion acoustic waves and hydrogen (H) cyclotron waves are unstable, with the former having much greater growth rates; He cyclotron waves are stable.

Certainly, as described in Sec. III, simulations show that the ion acoustic waves and H cyclotron waves are unstable. The former initially grow fastest. However, they quickly saturate to small amplitudes. The fundamental H cyclotron waves then begin to grow rapidly. In addition, after their saturation, the second harmonic H cyclotron waves are destabilized. Even though they are only marginally unstable in the initial state, they grow to the largest amplitudes. Because of the interactions with these waves, the electron parallel distribution function, $f_{\mathrm{e}}(v_\parallel)$, eventually has a large plateau region, ranging from the phase velocities of the ion acoustic waves to those of the second harmonic H cyclotron waves. Furthermore, the second harmonic waves heat He ions in the direction perpendicular to the magnetic field through cyclotron resonance. This heating is more significant than the heating of H.

We note that the heavy ion heating is sensitive to the electron temperature.[15,22] If, as in this article, T_{e} is much higher than T_{H}, then the frequencies of H cyclotron waves could be close to $(n+1/2)\Omega_{\mathrm{H}}$ (Ref. 23) (n denotes integer, while $n_{\mathrm{e}}, n_{\mathrm{H}}$ and n_{He} denote the densities of electrons, H, and He ions, respectively). Thus, the heavy ions with charge-to-mass ratio $Z_j/A_j \sim \frac{1}{2}$ (and therefore $\Omega_j \sim \Omega_{\mathrm{H}}/2$) could reso-

[a]Electronic mail: toida@phys.nagoya-u.ac.jp

nate with the H cyclotron waves; here, the subscript j refers to ion species.

Studies are often made under the assumption that T_e is much higher than T_i.[15,24] Such studies are meaningful because the temperature relaxation time between electrons and ions (τ_{ei}) is much longer than the relaxation times of electrons (τ_{ee}) and ions (τ_{ii}),

$$\tau_{ei}:\tau_{ee}:\tau_{ii}\sim m_i/m_e:\sqrt{m_i/m_e}:1, \tag{1}$$

where m_i and m_e are ion and electron masses, respectively. Observationally, for instance, the presence of very hot electrons is suggested in the loop-top hard x-ray sources in some solar flares.[25] Also, fluxes of electrons with a broad energy distribution are sometimes observed in the Earth's ionosphere.[14]

A summary and discussion of our work is given in Sec. IV. The present result indicates that the waves that are predicted to be stable by the linear theory based on the initial conditions can grow due to the change in the velocity distribution functions. These waves can strongly influence the energy transport. Also, because of the resonances with several different modes, a velocity distribution function can be deformed for a large velocity region. Evidently, the linear theory alone cannot predict these effects.

II. LINEAR THEORY

We analyze current-driven instabilities in a plasma consisting of H, He, and electrons. We assume that the ions have isotropic Maxwellian velocity distribution functions at $t=0$, and the electrons drift along the magnetic field $\boldsymbol{B}$; the initial electron distribution function may be written as

$$F_{e0}(v_\parallel,v_\perp)=\frac{1}{(2\pi v_{Te}^2)^{3/2}}\exp\left(-\frac{v_\perp^2}{2v_{Te}^2}\right)g(v_\parallel), \tag{2}$$

which is normalized so that $\int F_{e0}d^3v=1$. The subscript $\parallel$ and $\perp$ denote quantities parallel and perpendicular to the magnetic field, respectively; $g(v_\parallel)$ is the parallel distribution function.

Then, from the set of Vlasov equation and Gauss's law, the linear dispersion relations of electrostatic waves are given as[26,27]

$$1+\sum_{j=\mathrm{H,He}}\frac{1}{k^2\lambda_{Dj}^2}\left[1+\sum_{n=-\infty}^{\infty}\frac{\omega}{\sqrt{2}k_\parallel v_{Tj}}Z\left(\frac{\omega-n\Omega_j}{\sqrt{2}k_\parallel v_{Tj}}\right)\Gamma_n(\mu_j)\right]+\frac{\omega_{pe}^2}{k^2}\sum_{n=-\infty}^{\infty}\int d\boldsymbol{v}\left(\frac{n\Omega_e}{v_\perp}\frac{\partial F_{e0}}{\partial v_\perp}+k_\parallel\frac{\partial F_{e0}}{\partial v_\parallel}\right)\times\frac{J_n^2(\mu_e)}{k_\parallel v_\parallel-(\omega-n\Omega_e)}=0, \tag{3}$$

where the subscripts j and e refer to the ion species and the electrons, respectively; k is the wave number; λ_{Dj} is the Debye length; ω is the complex frequency; Ω_j is the cyclotron frequency ($\Omega_e<0$); ω_{pe} is the electron plasma frequency; and Z is the plasma dispersion function defined as[28]

$$Z(\xi)=\frac{1}{\sqrt{\pi}}\int_{-\infty}^{\infty}dx\frac{\exp(-x^2)}{x-\xi}. \tag{4}$$

Also, J_n is the Bessel function of the nth order, and $\Gamma_n(\mu_j)$ is $\Gamma_n(\mu_j)=I_n(\mu_j)\exp(-\mu_j)$, where I_n is the modified Bessel function of the nth order. The quantity μ_j is defined as $\mu_j=k_\perp^2\rho_j^2$ with ρ_j being the gyro-radius, $\rho_j=v_{Tj}/|\Omega_j|$.

We can analytically find linear growth rates of ion acoustic waves and H cyclotron waves under the assumptions that

$$|\omega-n\Omega_j|/(k_\parallel v_{Tj})\gg 1,\quad |\Omega_e|/(k_\parallel v_{Te})\gg 1. \tag{5}$$

If we retain the lowest-order ($n=0$) terms of electrons and ions in Eq. (3), we obtain the growth rates of ion acoustic waves as

$$\gamma\simeq\frac{\omega_r^3\sqrt{\pi}}{k_\parallel^2\Sigma_{j=\mathrm{H,He}}\omega_{pj}^2\Gamma_0(\mu_j)}\left[\frac{v_{Te}}{\lambda_{De}^2}\frac{\partial g}{\partial v_\parallel}\bigg|_{v_\parallel=\omega_r/k_\parallel}-\sum_{j=\mathrm{H,He}}\frac{1}{\lambda_{Dj}^2}\frac{\omega\Gamma_0(\mu_j)}{k_\parallel v_{Tj}}\exp\left(-\frac{\omega_r^2}{2k_\parallel^2v_{Tj}^2}\right)\right], \tag{6}$$

where ω_r is the real part of ω. The first and second terms represent the inverse Landau damping due to electrons and the ion Landau damping due to H and He, respectively. When the ion Landau damping is negligible, the growth rate is proportional to $\partial g/\partial v_\parallel$ at $v_\parallel=\omega_r/k_\parallel$.

Retaining the $n=0$ term of the electrons, the nth term of H, and n'th term of He in Eq. (3), we find the growth rates for H cyclotron waves

$$\gamma\simeq\frac{(\omega_r-n\Omega_H)^2\lambda_{DH}^2}{\omega_r\Gamma_n(\mu_H)\alpha}\left[\frac{v_{Te}}{\lambda_{De}^2}\frac{\partial g}{\partial v_\parallel}\bigg|_{v_\parallel=\omega_r/k_\parallel}-\frac{1}{\lambda_{DH}^2}\frac{\omega_r\Gamma_n(\mu_H)}{k_\parallel v_{TH}}\exp\left(-\frac{(\omega_r-n\Omega_H)^2}{2k_\parallel^2v_{TH}^2}\right)-\frac{1}{\lambda_{DHe}^2}\frac{\omega_r\Gamma_{n'}(\mu_{He})}{k_\parallel v_{THe}}\exp\left(-\frac{(\omega_r-n'\Omega_{He})^2}{2k_\parallel^2v_{THe}^2}\right)\right]. \tag{7}$$

Here, α is defined as

$$\alpha=1+\frac{\Gamma_{n'}(\mu_{He})}{\Gamma_n(\mu_H)}\frac{\lambda_{DH}}{\lambda_{DHe}}\frac{(\omega_r-n\Omega_H)^2}{(\omega_r-n'\Omega_{He})^2}, \tag{8}$$

which reduces to unity when $n_{He}=0$. The second and third terms in Eq. (7) represent the damping due to cyclotron resonances of H and He, respectively. The growth rates of H cyclotron waves are also proportional to $\partial g(v_\parallel)/\partial v_\parallel$ at $v_\parallel=\omega_r/k_\parallel$, if the cyclotron damping is negligible.

III. SIMULATION

A. Method and parameters

We study the nonlinear evolution of current-driven instabilities and associated energy transport in a multi-ion-species plasma, using a two-dimensional (two space and three velocity components), electrostatic particle code with full ion electron dynamics;[29] i.e., we use a nonrelativistic equation of

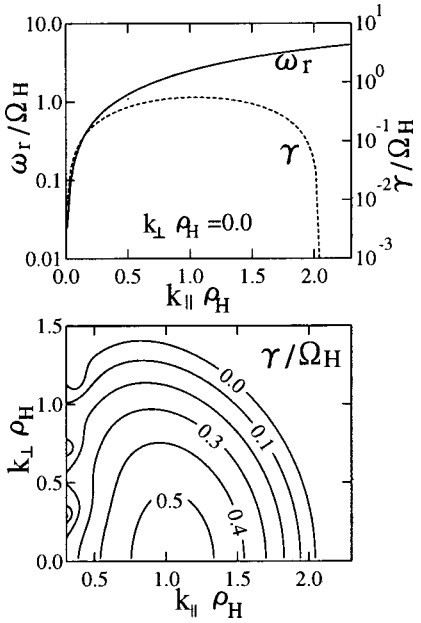

FIG. 1. Dispersion relations of ion acoustic waves. In the upper panel, the frequency ω_r and the growth rate γ of parallel ion acoustic waves ($k_\perp = 0$) are plotted as functions of $k_\parallel$. In the lower panel, a contour map of γ in the $(k_\parallel, k_\perp)$ plane is shown.

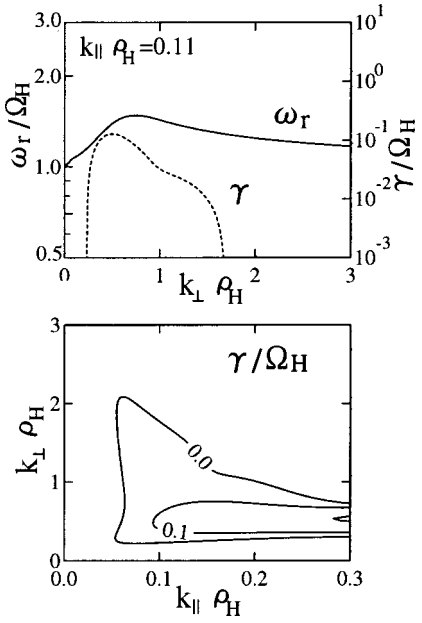

FIG. 2. Dispersion relations of fundamental H cyclotron waves. The upper panel shows ω_r and growth rate γ as functions of $k_\perp$ for $k_\parallel \rho_H = 0.11$, while the lower panel shows a contour map of γ in the $(k_\parallel, k_\perp)$ plane.

motion for particles and use Gauss's law for electric fields. The system size is $L_x \times L_y = 128\Delta_g \times 256\Delta_g$, where Δ_g is the grid spacing. We use periodic boundary conditions. The code has three particle species; H, He and electrons. Their total numbers are $N_H = 6\,946\,816$, $N_{He} = 720\,896$, and $N_e = 8\,388\,608$. The mass ratios are $m_H/m_e = 100$, $m_{He}/m_H = 4$; the charge ratios are $q_H/|q_e| = 1$ and $q_{He}/q_H = 2$; the temperature ratios are $T_e/T_H = 5.0$ and $T_{He}/T_H = 1$; the electron cyclotron frequency is $|\Omega_e|/\omega_{pe} = 2.0$. The Debye length is $\lambda_{De} = \Delta_g$. The time step Δt is $\omega_{pe}\Delta t = 0.15$. The external magnetic field is in the y direction. Given these parameters, the system covers the wave numbers $0 \leqslant k_\parallel \rho_H \leqslant 14$ and $0 \leqslant k_\perp \rho_H \leqslant 14$ with the spacing $\Delta(k_\parallel \rho_H) = 0.055$ and $\Delta(k_\perp \rho_H) = 0.11$ in $\boldsymbol{k}$ space.

For these parameters, the simulations are stable against numerical instabilities.[30] The total energy in the simulation is conserved; its change from $\omega_{pe} t = 0$ to 3000 is only 0.05%.

B. Dispersion relations for simulation parameters

Initially, the electrons have a shifted Maxwell distribution, Eq. (2) with

$$g(v_\parallel) = \exp[-(v_\parallel - v_d)^2/2v_{Te}^2]. \tag{9}$$

The drift speed is taken to be $v_d = v_{Te}$. For these initial conditions and parameters, we numerically solve Eq. (3), retaining terms from $n = 0$ to 10 for all the ion species and electrons. It is found that ion acoustic waves and H cyclotron waves are unstable, while He cyclotron waves are stable.

Figure 1 shows linear dispersion relations of the ion acoustic waves. In the upper panel, the frequency ω_r and the growth rate γ of the wave propagating parallel to the magnetic field ($k_\perp = 0$) are plotted as functions of the wave number $k_\parallel$. The lower panel shows a contour map of γ in the $(k_\parallel, k_\perp)$ plane. The mode with $k_\parallel \rho_H = 1.1$ and $k_\perp \rho_H = 0$ has the greatest growth rate; $\gamma = 0.5\Omega_H$ with $\omega_r = 2.7\Omega_H$.

The fundamental ($n = 1$) and second ($n = 2$) harmonic H cyclotron waves are unstable. Their growth rates, however, are smaller than those of the ion acoustic waves. Figure 2 shows dispersion relations of the fundamental H cyclotron waves. The upper panel shows ω_r and γ as functions of the perpendicular wave number $k_\perp$ ($k_\parallel$ is fixed to be $k_\parallel \rho_H = 0.11$). The mode with $k_\perp \rho_H = 0.5$ has the largest growth rate, $\gamma = 0.13\Omega_H$, with the frequency $\omega_r = 1.4\Omega_H$. Contour lines of γ in the $(k_\parallel, k_\perp)$ plane are plotted in the lower panel. The growth rate γ has large values when $k_\perp \rho_H \simeq 0.5$ and $k_\parallel \rho_H \gtrsim 0.1$.

Figure 3 shows dispersion relations of the second harmonics; in the upper panel, ω_r and γ are plotted for the waves with $k_\parallel \rho_H = 0.11$. The lower panel shows a contour map of γ. The growth rates are low and the unstable region is small, compared with the ion acoustic waves and the fundamental H cyclotron waves. We note that the wave with wave number $(k_\parallel \rho_H, k_\perp \rho_H) = (0.11, 0.75)$ is almost stable, with a very small growth rate $\gamma = 0.008\Omega_H$. It will be shown later by simulations, however, that this mode eventually develops into a dominant one.

C. Evolution of waves

In this subsection, we study the nonlinear evolution of the ion acoustic waves, fundamental and second harmonic H cyclotron waves. It will be shown that the ion acoustic waves initially grow fastest. However, they quickly saturate to small amplitudes. The fundamental H cyclotron waves then begin to grow rapidly. After their saturation, the second harmonics are destabilized; they grow to the largest amplitudes, even though they are only marginally unstable in the linear theory based on the initial conditions.

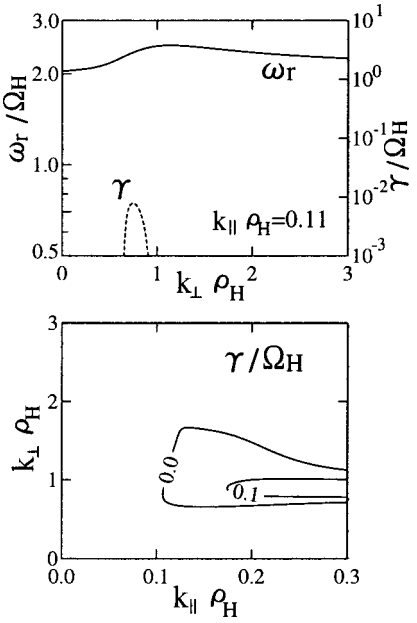

FIG. 3. Dispersion relations of second harmonic H cyclotron waves.

Figure 4 shows typical time evolution of an ion acoustic wave and two different H cyclotron waves. Here, the electric field energies $|E_k|^2$ are normalized to $m_e v_{Te}^2$ and are averaged over the time period $\omega_{pe}t=24$. The dotted line (a) represents an ion acoustic wave with the wave number $(k_\parallel \rho_H, k_\perp \rho_H)=(0.94,\ 0.11)$. The dashed line (b) and solid line (c) show H cyclotron waves with $(k_\parallel \rho_H, k_\perp \rho_H)=(0.11,\ 0.55)$ and (0.11, 0.77), respectively. We will refer to these modes as modes (a), (b) and (c), respectively. In the early stage, the ion acoustic wave (a) grows fastest. The observed initial growth rate, $\gamma \simeq 0.48\Omega_H$, is in good agreement with the theoretical prediction, $\gamma=0.52\Omega_H$. However, this mode is quickly saturated and is damped after the time $\omega_{pe}t \simeq 150$. In the beginning, mode (b) grows slowly. However, at $\omega_{pe}t \simeq 300$, it begins to grow with a larger growth rate, $\gamma \simeq 0.45\Omega_H$, than the theoretical value $\gamma=0.13\Omega_H$ obtained from the initial velocity distribution functions. The saturation occurs at $\omega_{pe}t \simeq 600$, which is followed by the amplitude

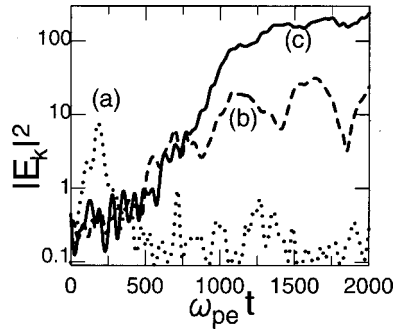

FIG. 4. Time variation of $|E_k|^2$ of an ion acoustic wave and two H cyclotron waves. The dotted line (a) shows an ion acoustic wave with $(k_\parallel \rho_H, k_\perp \rho_H)=(0.94,0.11)$. The dashed line (b) and the solid line (c) represent H cyclotron waves with $(k_\parallel \rho_H, k_\perp \rho_H)=(0.11,\ 0.55)$ and (0.11, 0.77), respectively. Here, $|E_k|^2$ is normalized to $m_e v_{Te}^2$ and is averaged over the time period $\omega_{pe}t=24$.

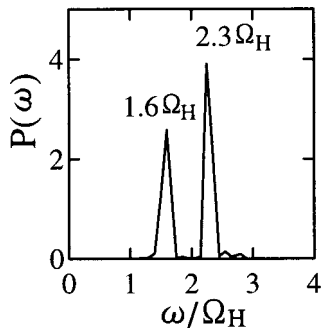

FIG. 5. Frequency spectrum for mode (b).

oscillation with a period $\omega_{pe}t \simeq 440$. Finally, at $\omega_{pe}t \simeq 600$, mode (c) starts to grow rapidly; the observed growth rate during the period from $\omega_{pe}t=600$ to $\omega_{pe}t=1{,}000$ is $\gamma \simeq 0.2\Omega_H$. The growing continues until the time $\omega_{pe}t \simeq 1500$. Even though mode (c) is only marginally unstable in the initial state, its amplitude eventually becomes much larger than those of modes (a) and (b).

Figure 5 shows a frequency spectrum for mode (b) obtained from the x component of the electric field for the period from $\omega_{pe}t=0$ to 3000. There are two peaks due to fundamental and second harmonic H cyclotron waves, respectively. The latter is initially stable but is eventually destabilized by the change in the electron velocity distribution function. The amplitude oscillation of mode (b), which was shown in Fig. 4, is caused by the beating between the fundamental and the second harmonic waves. The frequency spectrum for mode (c) is shown in Fig. 6. The peak is formed by the second harmonic H cyclotron wave; its frequency $\omega \simeq 2.4\Omega_H$ is in good agreement with the theoretical value $\omega=2.3\Omega_H$.

In Figs. 4–6, we investigated the development of three typical modes. We now discuss the evolution of many different modes. Figure 7 shows distributions of $|E_k|^2$ in the $(k_\parallel, k_\perp)$ plane at $\omega_{pe}t=600$, 1800, 3000, and 4800. The size of a filled circle represents the magnitude of the field energy, $|E_k|^2$, of a mode $(k_\parallel, k_\perp)$. At $\omega_{pe}t=600$, the fundamental H cyclotron mode $(k_\parallel \rho_H, k_\perp \rho_H)=(0.22,\ 0.66)$ has the largest energy. Then, at $\omega_{pe}t=1800$, the modes with smaller $k_\parallel$ are growing, and mode (c) has the greatest energy. It remains the dominant mode after this time. The modes $(\pm 0.11,\ 0.66)$ and $(\pm 0.11,\ 0.88)$ are the second harmonic H cyclotron waves,

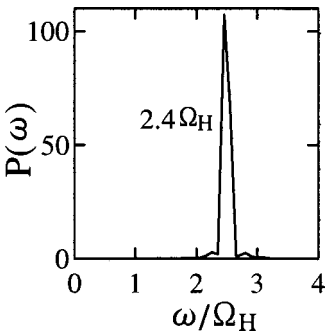

FIG. 6. Frequency spectrum for mode (c).

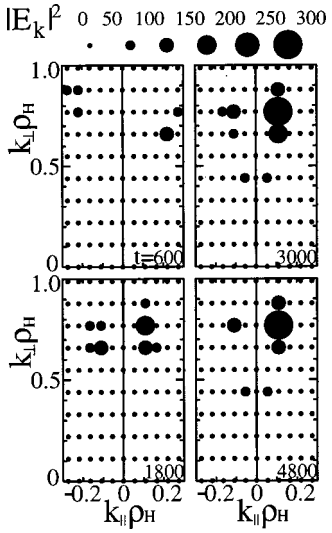

FIG. 7. Distributions of $|E_k|^2$ in the $(k_\parallel, k_\perp)$ plane at $\omega_{pe}t=600$, 1800, 3000, and 4800. The magnitude of $|E_k|^2$, normalized to $m_e v_{Te}^2$, is shown of a filled circle.

while the modes (± 0.055, 0.44) are the fundamental H cyclotron waves. Note that the most unstable ion acoustic waves have $k_\parallel \rho_H \sim 1$ and are not shown here.

D. Evolution of electron distribution

The waves and electron velocity distribution functions strongly affect each other. It will be shown here that the instabilities of three kinds of waves with different phase velocities give rise to flattening of the electron distribution function over a wide velocity region.

Figure 8 shows evolution of the distribution function for parallel electron velocity; because ***B*** is in the *y* direction, it is defined as

$$f_e(v_\parallel) \equiv N_e \int F_e dv_x dv_z dx dy. \tag{10}$$

The left panel shows its overall profiles at $\omega_{pe}t=0$ and 3000, while the right one gives its expanded views at various times.

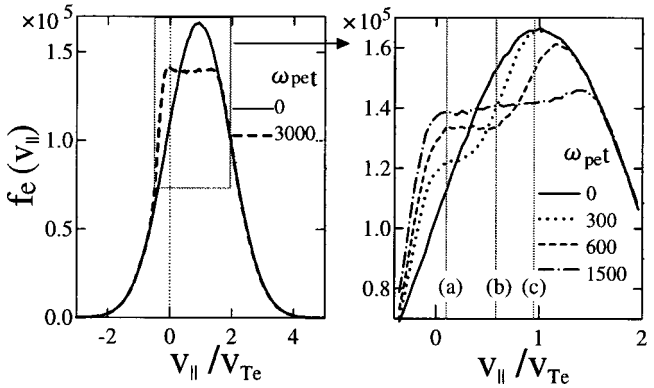

FIG. 8. Evolution of the distribution function for parallel electron velocity, $f_e(v_\parallel)$. The overall profiles at $\omega_{pe}t=0$ and 3000 are plotted in the left panel. Its expanded views at $\omega_{pe}t=0$, 300, 600, and 1500 are plotted in the right panel. Three vertical lines (a), (b), and (c) represent parallel phase velocities of modes (a), (b), and (c), respectively.

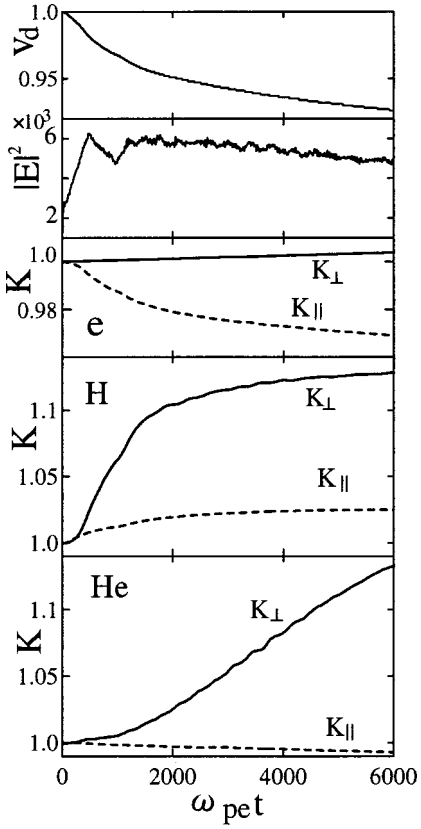

FIG. 9. Time variations of electron drift speed, total electric field energy, and total kinetic energies of electron, H, and He. Electron drift speed, electric field energy, and kinetic energies are normalized to v_{Te}, $m_e v_{Te}^2$, and initial kinetic energies, respectively.

The vertical lines (a), (b), and (c) show parallel phase velocities, $\omega/k_\parallel$, of the ion acoustic wave ($\omega/k_\parallel = 0.11 v_{Te}$), fundamental H cyclotron wave ($\omega/k_\parallel = 0.57 v_{Te}$), and second harmonic wave ($\omega/k_\parallel = 0.97 v_{Te}$), respectively. Initially, $f_e(v_\parallel)$ is a shifted Maxwellian. However, it is gradually deformed to have a plateau in the region, $0 \lesssim v_\parallel/v_{Te} \lesssim 1.5$. Inspection of the right panel (and Fig. 4) indicates that the ion acoustic waves, which have the lowest phase velocities, grow first. This flattens $f_e(v_\parallel)$ around their phase velocities, i.e., around line (a), and makes the slope steep around line (b). Then, the fundamental cyclotron waves grow and make the slope of $f_e(v_\parallel)$ flat around line (b) and steep around line (c). Finally, the second harmonics are destabilized, making $f_e(v_\parallel)$ flat around line (c). In this way, $f_e(v_\parallel)$ has a large plateau region, ranging from the phase velocities of the ion acoustic waves to those of the second harmonic H cyclotron waves. After the saturation of mode (c), rapid growing modes were not observed in this simulation.

E. Ion heating

Heavy-ion heating perpendicular to the magnetic field is observed in the simulations. It is caused by cyclotron resonance with the second harmonic H cyclotron waves. Figure 9 displays time variations of the electron drift speed (parallel velocity averaged over all the electrons), total electric field energy, and kinetic energies of electrons, H and He ions; the solid and dashed lines in the lower three panels represent

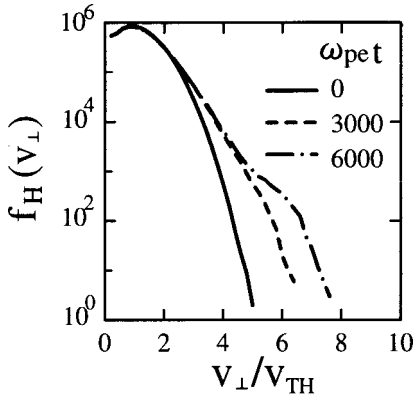

FIG. 10. Perpendicular hydrogen velocity distribution, $f_H(v_\perp)$, at $\omega_{pe}t=0$, 3000, and 6000.

perpendicular energy $K_\perp$ and parallel energy $K_\parallel$, respectively. Here, the electron drift speed, electric field energy, and kinetic energies are normalized to v_{Te}, $m_e v_{Te}^2$, and initial kinetic energies, respectively. The electron drift speed gradually decays with time. The parallel kinetic energy of electrons is transferred to the ion kinetic energies through the unstable waves. In both H and He ions, $K_\perp$ increases much more than $K_\parallel$. ($K_\parallel$ of He ions is almost constant. Its change is less than 1% in this simulation.) After $\omega_{pe}t\sim 1{,}500$, $K_\perp$ of He ions continues to increase more rapidly than that of H ions. As we will see later, both H and He are heated by cyclotron resonances. (The fast increase in $K_\perp$ of H in the initial phase, $\omega_{pe}t\lesssim 1500$, is due to collective motions forming the unstable waves.)

We show in Fig. 10 distribution functions $f_H(v_\perp)$ for H ions at various times. Also, we show in Fig. 11 distribution functions $f_{He}(v_\perp)$ for He. Recall the total number of H ions is ten times as large as that of He. The number of high-energy particles increases with time. It is especially significant in He ions in high energy regime such that $v_\perp/v_{THe}\gtrsim 5$.

Figure 12 shows contour maps of the hydrogen distribution function $f_H(v_\parallel,v_\perp)$ at three different times. The particles with $v_\parallel/v_{TH}\simeq 4.0$ are heated perpendicularly. These particles satisfy the resonance condition, $\omega-2\Omega_H-k_\parallel v_\parallel\simeq 0$, with mode (c) ($\omega=2.4\Omega_H$, $k_\parallel\rho_H=0.11$, and

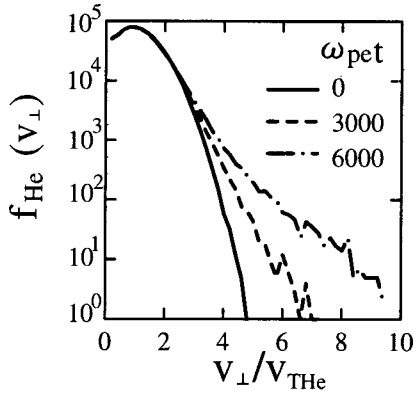

FIG. 11. Perpendicular helium velocity distribution, $f_{He}(v_\perp)$, at various times.

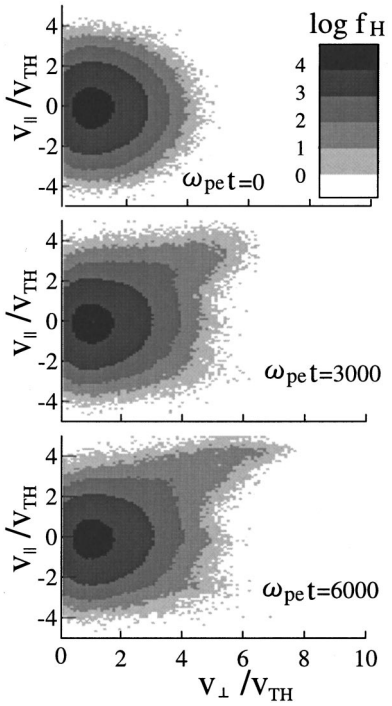

FIG. 12. Contour maps of $f_H(v_\parallel,v_\perp)$ at $\omega_{pe}t=0$, 3000, and 6000.

$k_\perp\rho_H=0.77$). The resonance occurs in the tail of the parallel velocity distribution. The slow increase in $K_\perp$ of H ions after the time $\omega_{pe}t\simeq 1500$ shown in Fig. 9 is due to this process. Figure 13 shows contour maps of the helium distribution function, $f_{He}(v_\parallel,v_\perp)$. The particles with $v_\parallel/v_{THe}\simeq 0.65$ are heated by the same wave, mode (c), through the resonance, $\omega-5\Omega_{He}-k_\parallel v_\parallel\simeq 0$. Because the resonance takes place in

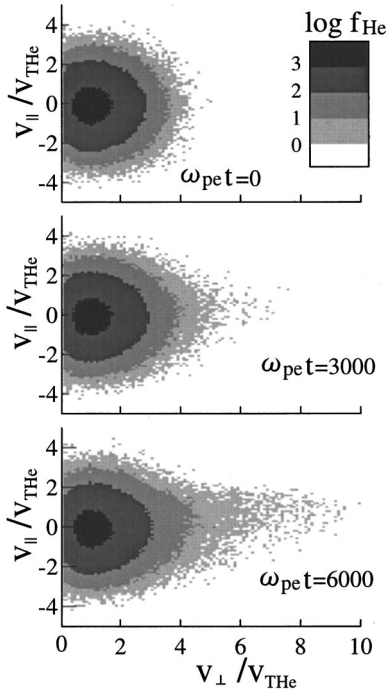

FIG. 13. Contour maps of $f_{He}(v_\parallel,v_\perp)$ at various times.

the region of small parallel velocity, the time rate of change in $K_\perp$ of He is much greater than that of H for $\omega_{pe}t \gtrsim 1500$ as expected from Eq. (7).

IV. DISCUSSION AND SUMMARY

We have studied current-driven instabilities in a two-ion-species plasma using the particle simulation, with special attention to energy transport among different particle species through unstable waves.

We considered a plasma consisting of H, He, and electrons with the density ratio, $n_{He}/n_H = 0.1$. The electron temperature was taken to be higher than the ion temperature, $T_e = 5T_H$. The initial electron drift speed parallel to the magnetic field was equal to the electron thermal speed. For the initial simulation parameters, the linear theory predicts that ion acoustic waves and H cyclotron waves are unstable, while He cyclotron waves are stable. The ion acoustic waves have larger growth rates than H cyclotron waves.

We then solved the initial value problem of this system by using a two-dimensional, electrostatic particle code with full ion and electron dynamics. The evolution of waves is strongly affected by the shape of the electron parallel velocity distribution function, $f_e(v_\parallel)$, which is likewise changed by the unstable waves. Initially, ion acoustic waves grow fastest and deform $f_e(v_\parallel)$ around their phase velocities. The change in $f_e(v_\parallel)$ stabilizes ion acoustic waves and enhances growing of fundamental H cyclotron waves. These cyclotron waves then flatten $f_e(v_\parallel)$ near their phase velocities. This destabilizes the second harmonics. Even though the second harmonics are only marginally unstable in the initial state, they eventually grow to the largest amplitudes. They again deform $f_e(v_\parallel)$ around their phase velocities. As a result, $f_e(v_\parallel)$ has a flat profile over a wide velocity region.

The second harmonics heat He ions perpendicular to the magnetic field through cyclotron resonance. The helium was observed to be heated more than the hydrogen. This is because He ions have resonances at velocities lower than their thermal velocity, while the resonance of H ions occurs at velocities much higher than their thermal velocity.

The fact that He ions are heated more than H ions is not expected by the linear theory based on the initial conditions. In fact, the parallel phase velocities of the most unstable ion acoustic wave are much higher than the thermal speed of He; $\omega/k_\parallel \simeq 2.5v_{TH} = 5v_{THe}$. Hence, He ions cannot resonate with the ion acoustic waves. Heating of He ions occurs after the second harmonic cyclotron waves are destabilized. This indicates that the linear theory cannot predict which particle species are heated. We must develop a theory which self-consistently treats the evolution of waves and velocity distribution functions. Then, we would be able to account for the energy transport among different particle species in the solar corona or in the Earth's ionosphere.

ACKNOWLEDGMENT

This work was carried out by the joint research program of the Solar-Terrestrial Environment Laboratory, Nagoya University.

[1] J. P. Meyer, Astrophys. J., Suppl. Ser. **57**, 151 (1985).
[2] J. P. Meyer, Astrophys. J., Suppl. Ser. **57**, 173 (1985).
[3] M. Toida and Y. Ohsawa, J. Phys. Soc. Jpn. **64**, 2036 (1995).
[4] M. Toida and Y. Ohsawa, Sol. Phys. **171**, 161 (1997).
[5] O. A. Shaeffer and J. Zähringer, Phys. Rev. Lett. **8**, 389 (1962).
[6] J. D. Anglin, Astrophys. J. **198**, 733 (1975).
[7] D. V. Reames, Astrophys. J. **73**, 235 (1990).
[8] D. V. Reames, J. P. Meyer, and T. T. von Rosenvinge, Astrophys. J., Suppl. Ser. **90**, 649 (1994).
[9] G. J. Hurford, R. A. Mewaldt, E. C. Stone, and R. E. Vogt, Astrophys. J. Lett. **201**, L95 (1975).
[10] G. M. Mason, L. A. Fisk, D. Hovestadt, and G. Gloeckler, Astrophys. J. **239**, 1070 (1980).
[11] G. M. Mason, D. V. Reames, B. Klecker, D. Hovestadt, and T. T. von Rosenvinge, Astrophys. J. **303**, 849 (1986).
[12] E. G. Shelly, R. D. Sharp, and R. G. Johnson, Geophys. Res. Lett. **3**, 654 (1976).
[13] P. M. Kinter, J. Vago, S. Chesney, R. L. Arnoldy, K. A. Lynch, C. J. Pollock, and T. E. Moore, Phys. Rev. Lett. **68**, 2448 (1992).
[14] M. André, P. Norqvist, L. Andersson, L. Eliasson, A. I. Eriksson, L. Blomberg, R. E. Erlandson, and J. Waldemark, J. Geophys. Res. **103**, 4199 (1998).
[15] L. A. Fisk, Astrophys. J. **224**, 1048 (1978).
[16] T. X. Zhang, M. Toida, and Y. Ohsawa, J. Phys. Soc. Jpn. **62**, 2545 (1993).
[17] T. X. Zhang and Y. Ohsawa, Sol. Phys. **158**, 115 (1995).
[18] S. Nakazawa, T. X. Zhang, and Y. Ohsawa, Sol. Phys. **166**, 159 (1996).
[19] H. Okuda, C. Z. Cheng, and W. W. Lee, Phys. Fluids **24**, 1060 (1981).
[20] M. Ashour-Abdalla and H. Okuda, J. Geophys. Res. **89**, 2235 (1984).
[21] M. Ashour-Abdalla, D. Schrier, and H. Okuda, J. Geophys. Res. **93**, 12826 (1988).
[22] P. J. Palmadesso, T. P. Coffey, S. L. Ossakow, and K. Papadopoulos, Geophys. Res. Lett. **1**, 105 (1974).
[23] J. M. Kindel and C. F. Kennel, J. Geophys. Res. **76**, 3055 (1971).
[24] B. D. Fried and R. W. Gould, Phys. Fluids **4**, 139 (1961).
[25] S. Tsuneta, S. Masuda, T. Kosugi, and J. Sato, Astrophys. J. **478**, 787 (1997).
[26] W. E. Drummond and M. N. Rosenbluth, Phys. Fluids **5**, 1507 (1962).
[27] T. H. Stix, *Waves in Plasmas* (AIP, New York, 1992).
[28] B. D. Fried and S. D. Conte, *The Plasma Dispersion Function* (Academic, New York, 1961).
[29] J. M. Dawson, Rev. Mod. Phys. **55**, 403 (1983).
[30] A. B. Langdon, J. Comput. Phys. **6**, 247 (1970).